energies

MDPI

Article

An Analytical and Numerical Study of Magnetic Spring Suspension with Energy Recovery Capabilities

Yu Jia [1,*], Shasha Li [2] and Yu Shi [1,*]

[1] Department of Mechanical Engineering, Thornton Science Park, University of Chester, Chester CH1 4BJ, UK

[2] Department of Mechanical Invention Examination, China National Intellectual Property Administration, Beijing 100088, China; lishasha@sipo.gov.cn

* Correspondence authors: yu.jia.gb@ieee.org (Y.J.); y.shi@chester.ac.uk (Y.S.)

Received: 18 October 2018; Accepted: 10 November 2018; Published: 12 November 2018

Abstract: As the automotive paradigm shifts towards electric, limited range remains a key challenge. Increasing the battery size adds weight, which yields diminishing returns in range per kilowatt-hour. Therefore, energy recovery systems, such as regenerative braking and photovoltaic cells, are desirable to recharge the onboard batteries in between hub charge cycles. While some reports of regenerative suspension do exist, they all harvest energy in a parasitic manner, and the predicted power output is extremely low, since the majority of the energy is still dissipated to the environment by the suspension. This paper proposes a fundamental suspension redesign using a magnetically-levitated spring mechanism and aims to increase the recoverable energy significantly by directly coupling an electromagnetic transducer as the main damper. Furthermore, the highly nonlinear magnetic restoring force can also potentially enhance rider comfort. Analytical and numerical models have been constructed. Road roughness data from an Australian road were used to numerically simulate a representative environment response. Simulation suggests that 10's of kW to >100 kW can theoretically be generated by a medium-sized car travelling on a typical paved road (about 2–3 orders of magnitude higher than literature reports on parasitic regenerative suspension schemes), while still maintaining well below the discomfort threshold for passengers (<0.315 m/s^2 on average).

Keywords: magnetic spring; suspension; energy recovery

1. Introduction

In recent years, there has been a rapidly growing interest in the transition fossil fuel-based automotive vehicles towards hybrid and electric vehicles (EVs) in order to minimise carbon emissions, curb pollution and mitigate climate change [1]. The development of EVs has been strongly supported by the automotive industry and driven by governmental policy in many countries. For instance, the French government plans to stop the sale of all greenhouse gas-emitting vehicles by 2040 [2]; the UK government aims to ban the sale of new fossil fuel vehicles from 2040 onwards and outlaw the use of all such vehicles on British roads from 2050 onwards [3]; Scotland plans to phase out petrol and diesel cars by 2032 [4]; and there are similar initiatives planned in Austria, China, Denmark, Germany, India, Ireland, Japan, Norway, the Netherlands, Portugal, South Korea and Spain [5].

However, despite the motivation to shift towards EVs, a key persisting challenge is the limited range of travel possible from a full charge, which can be several times less than equivalent fossil fuel cars with a full tank of fuel [6]. As battery capacity increases, the added weight results in a diminishing return in terms of the range added per kilowatt-hour. For instance, while the Nissan Leaf MY 2016 has a range of up to 172 km with a 24-kWh battery (7.2 km/kWh), the 100-kWh version of the Tesla Model

S only increases the maximum range to 550 km (reduced to 5.5 km/kWh) [7]. There is increasing EV battery research [8] aiming to improve energy density, reduce weight and cost, as well as improve the reliability in potentially harsh operating environments associated with automotive applications. However, it is recognised that the current generation of lithium-based battery technologies on their own is insufficient to enable EVs to replace the mass market fossil fuel cars entirely [8].

On the other hand, the inclusion of vehicle energy recovery systems within EVs can help to bridge the technological gap by recharging the onboard battery and extending range between hub charge cycles [9]. Examples of some of the relatively more well-established vehicle energy recovery systems include: fuel cells, photovoltaic cells, thermoelectric generators and regenerating braking systems [9]. Each of these power generation technologies have attracted immense interest from the automotive industry and academic researchers in recent years. However, none of these are practically capable of substantially extending the mileage range of EVs due to the relatively low power recovered compared to the capacity of automotive batteries.

In addition to the above-mentioned vehicle energy recovery strategies, a substantial amount of kinetic energy is also present within the vehicle suspension system [10,11]. The suspension aims to dampen the vibration experienced by the body of the vehicle above the wheel and suspension (unsprung mass of the vehicle). Vibration is induced as vehicles are unavoidably excited by road irregularities such as bumps, pavement imperfections, surface cracks, pot holes, as well as braking and acceleration forces. The damping of this vibrational energy by the suspension system is crucial to ensure minimal vibration is passed onto the unsprung mass in order to minimise any adverse affects on the passenger comfort and experience, vehicle handling and manoeuvrability, safety and potential damage to the vehicle [12,13].

Modern automotive suspension systems typically consist of a physical spring made up of either a mechanical spring, a hydraulic spring or a pneumatic spring. The physical springs are electrically controlled by either an active or semi-active suspension control system [14,15]. The main bulk of the vibrational energy is dissipated in the physical springs, which are also electrically damped by various control methods [16–18] to improve vehicle dynamic behaviour, rider comfort and safety [19]. Nonlinear springs (higher order polynomial stiffness term), such as hydraulic or pneumatic, are beneficial in introducing higher restoring forces when the vibration amplitude becomes large.

There are a few studies to date on recovering energy from automotive suspension systems [20], which typically involve a conventional mechanical spring system [11] with added transducers such as electromagnetic [21] or piezoelectric [22], which parasitically extract energy from the primary spring system [23–25]. The transducers are typically intended to be retrofitted onto the suspension spring. Such a parasitic energy extraction approach can only generate an extremely small level of power compared to the power requirement of the EV powertrain [19]. Experimental studies generally report average power in the order of 10's of W [23,26], and theoretical predictions range from 10's of W [23,24] to 1's of kW [19,22]. Such power levels are several orders of magnitude lower than the 100's of kW power consumption required by EV's electric motors [7].

The fundamental problem with all of these existing reported suspension energy recovery approaches is that the majority of the vibrational energy is still primarily dissipated to the environment through the physical spring mechanism. The harvested energy is essentially derived from parasitic damping, which merely constitutes a small share of the overall damping within the spring shock-absorber system. This is not surprising, as the conventional suspension systems are not designed to accommodate electrical energy recovery and are optimised to dissipate energy to the environment.

Therefore, this paper proposes a fundamental redesign (outlined in Figure 1) of the automotive suspension in order to enable an efficient method for achieving regenerative suspension where a significant portion of the dissipated vibrational energy is converted into useful electrical energy. This is achieved by swapping the conventional physical spring mechanisms (such as mechanical spring, pneumatic spring or hydraulic spring) with permanent magnetic springs. The magnets directly form a

part of a large electromagnetic transducer, which acts as the primary damping mechanism. This directly couples vibrational energy to the electrical domain, rather than the parasitic harvesting schemes.

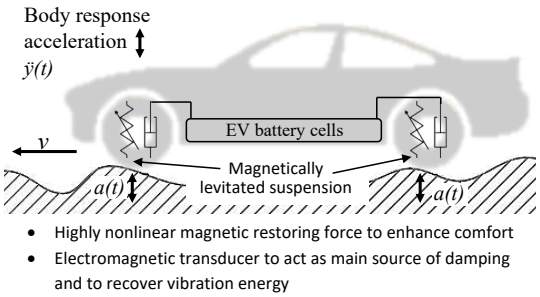

Figure 1. Concept of a car with a magnetic suspension and an electromagnetic energy recovery system while driving on rough roads.

Furthermore, the highly nonlinear restoring force of the magnetic spring can also potentially provide better comfort and vehicle handling compared to mechanical, pneumatic or hydraulic springs [27]. While there are some works on using electromagnetic transducers as part of a conventional suspension system to improve control and offer better ride comfort [21,28], this is the first study to propose the concept of a purely magnetically-levitated automotive suspension method, aimed at the purpose of enabling high power regenerative suspension.

2. Theory

2.1. Design

A quarter vehicle suspension model is illustrated in Figure 2. Figure 2a illustrates a conventional mass-spring-damper system. Mechanical springs generally have a linear restoring force for small displacement. At large displacements, geometric nonlinearity can result in a weakly nonlinear third order Duffing-type restoring force. On the other hand, pneumatic and hydraulic suspensions are inherently second order spring systems. The damper dissipates the majority of the energy, and a variable damper can be actively controlled for adaptive suspension. Figure 2b presents the proposed magnetic suspension system, where the magnet attached to the unsprung mass is magnetically levitated between a pair of top and bottom magnets. The magnetic restoring force is highly nonlinear, and the directly coupled electromagnetic transducer acts as the primarily damper.

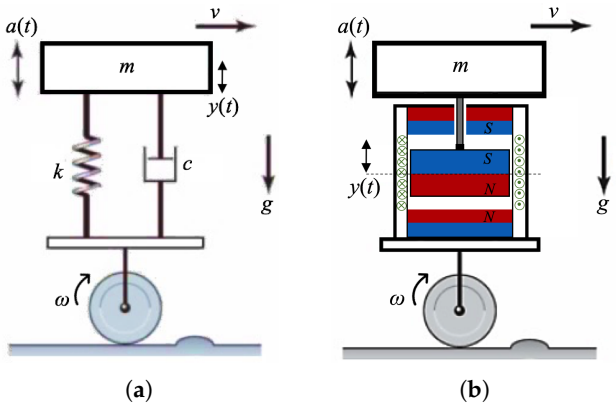

Figure 2. Quarter model of the car suspension. The sprung models of the inflated wheel and the seat are not shown here. The control system is also not shown here, which either varies the damping ratio of conventional springs or the electromagnetic coupling of the magnetic suspension. (**a**) Mechanical spring suspension; (**b**) magnetic spring suspension.

Figure 3 compares the restoring force of various spring systems. It can be seen that for very small displacements, all springs collapses to an approximately linear behaviour. Within 25% of normalised displacement, all higher order nonlinear springs are roughly equivalent as they outperform linear springs. However, at even higher displacements, the various higher orders starts to diverge. The magnetic spring can be seen to possess exceptionally high restoring force at larger displacements as the repulsive dipoles close on each other.

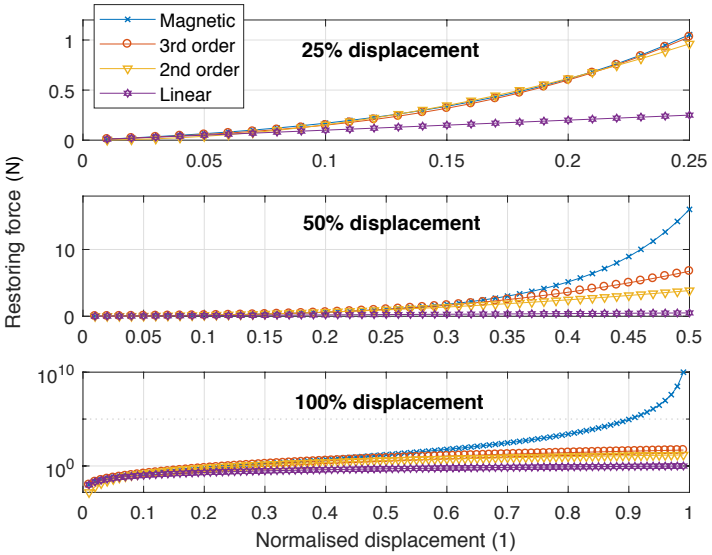

Figure 3. Restoring force of various orders of spring mechanisms. While a second order spring such as a pneumatic system or a third order spring such as a Duffing-type system offers relatively the same restoring force within a small displacement (∼25%), the magnetic spring has a significantly higher nonlinear restoring force at a larger displacement level. Therefore, magnetic springs can serve as a more effective suspension mechanism for large vibration scenarios.

The higher order nonlinear restoring force implies that larger displacements from high acceleration shocks can be effectively absorbed. A similar level of impulse force would therefore result in small response displacements in the unsprung mass sitting on top of a higher order nonlinear spring. Therefore, magnetic springs have the potential to provide better shock absorption and comfort levels than mechanical, pneumatic and hydraulic suspension systems.

2.2. Analytical

The magnetic spring force can be represented by Equation (1), which is an approximation of the dipole interaction two cylindrical magnets.

$$F_{mag}(y,t) = -\frac{\pi\mu_0 M^2 r^4}{4}\left[\frac{1}{y(t)^2} + \frac{1}{(y(t)+2h)^2} + \frac{2}{(y(t)+h)^2}\right] \quad (1)$$

where F_{mag} is the magnetic force between two cylindrical magnets, μ_0 is the permeability of free space (1.26×10^{-6} H/m), M is the magnetisation field ($M = B/\mu_0$), B is the flux density in Teslas, r is the radius of the magnet, h is the thickness of the magnet, y is the displacement and the distance between the magnets and t is the time domain.

When one magnet is fixed and the other is allowed to oscillate vertically above it (orientated for repulsion), utilising the magnetic spring, the motion of the oscillatory system can be written as in Equation (2).

$$m\frac{\mathrm{d}^2 y}{\mathrm{d}t^2} + c\frac{\mathrm{d}y}{\mathrm{d}t} + F_{mag}(y,t) - mg = F(t) \quad (2)$$

where m is the effective mass of the oscillating system (movable magnet plus the unsprung mass sitting on top of it), c is the total damping (including mechanical and electrical domains), g is the acceleration due to gravity and $F(t)$ is the external excitation force.

Critical damping c_c of the oscillator depends on the stiffness. However, as the stiffness is a displacement-dependent entity, so it is for the critical damping. The stiffness constant k, natural frequency $\omega_n(y,t)$, critical damping c_c and damping constant c can be expanded as shown in Equations (3)–(6), respectively.

$$k = \frac{F_{mag}(y,t)}{y(t)} \tag{3}$$

$$\omega_n(y,t) = \sqrt{\frac{F_{mag}(y,t)}{my(t)}} \tag{4}$$

$$c_c = 2m\sqrt{\frac{F_{mag}(y,t)}{my(t)}} \tag{5}$$

$$c = 2\zeta m\sqrt{\frac{F_{mag}(y,t)}{my(t)}} \tag{6}$$

It is important to note that the natural frequency is not fixed here, and it varies depending on the displacement y(t), which in turn is a function of time t. The system described so far is a movable magnet levitated above a fixed magnet. While there is restoring force on the movable magnet as it displaces towards the fixed magnet, there is no restoring force from the opposite direction.

In order to add a restoring force from above, a third magnet, fixed on the top, is thus needed. This can be represented by Equation (7), where a moving magnet sits between a pair of fixed magnets from above and below.

$$F_{magTop}(y,t) = \frac{\pi\mu_0 M^2 r^4}{4}\left[\frac{1}{(L-y(t))^2} + \frac{1}{(L-y(t)+2h)^2} + \frac{2}{(L-y(t)+h)^2}\right] \tag{7}$$

where L is the total spacing between the surfaces of two fixed magnets within which the movable magnet can oscillate.

The overall equation of motion of such a three-magnet system can therefore be summarised by Equation (8), and the damping constant is given by Equation (9).

$$m\frac{\mathrm{d}^2y}{\mathrm{d}t^2} + c\frac{\mathrm{d}y}{\mathrm{d}t} + F_{mag}(y,t) + F_{magTop}(y,t) - mg = F(t) \tag{8}$$

$$c = 2\zeta m\sqrt{\frac{F_{mag}(y,t) + F_{magTop}(y,t)}{my(t)}} \tag{9}$$

Therefore, the fully-expanded equation of motion for a magnet levitated between an upper fixed magnet and a lower fixed magnet is given by Equation (10).

$$\begin{aligned}\ddot{y} + 2\zeta\sqrt{\frac{F_{mag}(y,t) + F_{magTop}(y,t)}{my(t)}}\dot{y} - g \\ -\frac{\pi\mu_0 M^2 r^4}{4m}\left[\frac{1}{y^2} + \frac{1}{(y+2h)^2} + \frac{2}{(y+h)^2}\right] \\ +\frac{\pi\mu_0 M^2 r^4}{4m}\left[\frac{1}{(L-y)^2} + \frac{1}{(L-y+2h)^2}\right. \\ \left. +\frac{2}{(L-y+h)^2}\right] = a\cos(\omega t) + W(t)\end{aligned} \tag{10}$$

where a is the excitation acceleration amplitude, ω is the excitation angular frequency and W is the excitation noise intensity.

The total power transfer $P(t)$ possible from the source to the damping mechanism is given by the generic Equation (11).

$$P(t) = -ma(t)\left[\int a\ \mathrm{d}t\right] - ma(t)\dot{y}(t) \tag{11}$$

If a coil is wound around the magnetic springs, especially around the varying flux region of the movable magnet, an electromagnetic transducer can be achieved. Energy from the mechanical domain can then be fed into the electrical domain for electrical power generation; and vice versa, it is also possible for active or semi-active suspension control.

The damping is primarily formed by parasitic mechanical loss and electrical damping. For a matched load, up to half of the damping can be comprised of electrical damping [29]. Therefore, the effective damping ratio is given by Equation (12), and the maximum theoretical raw power recoverable can be represented by Equation (13).

$$\zeta = \zeta_m + \zeta_e + \zeta_p \tag{12}$$

where ζ_m is the mechanical damping ratio, ζ_e is the electrical damping ratio and ζ_p is the parasitic damping ratio. For an optimal impedance matched system, $\zeta_m \approx \zeta_e >> \zeta_p$. In the proposed system here, most of the energy recovery is achieved through ζ_e; whereas for most reported parasitic energy recovery approaches in the literature [22–24], energy is recovered through ζ_p.

$$P(t) = \frac{m\zeta_e\omega_n^3 y(t)^2}{4(\zeta_m + \zeta_e)} \tag{13}$$

In this proposed electromagnetic suspension system using permanent magnets as the restoring spring force, theoretically, up to half of the total energy can be dumped into the electrical domain. Including potential circuitry inefficiencies and the efficiency of maximum power tracking via variable electrical impedance matching, further loss in the electrical domain is to be expected. However, the recoverable power is significantly higher than retrofitting transducers on conventional suspensions, where only parasitic harvesting is possible.

3. Numerical Simulation

3.1. Method

A numerical model in MATLAB was constructed to simulate the derived analytical equations. The ODE45 numerical solver with variable time resolution was used. An overview of the model is outlined in Figure 4.

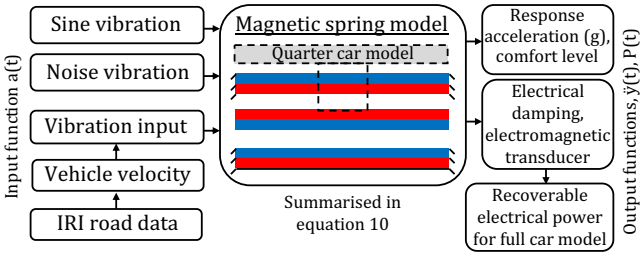

Figure 4. Overview of numerical model used to simulate the behaviour of the quarter vehicle magnetic suspension.

External excitations included the sinusoidal signal, band-limited noise and measured road condition data. As a starting point, a quarter vehicle magnetic suspension model, along with a 400-kg unsprung mass, was used. The magnet chosen was N52 NdFeB, which is currently amongst the highest strength commercially available magnets. The recoverable electrical power assumes a 50% loss in the transducer conversion for optimal impedance matching as outlined by Equation (13), 90% efficiency for a typical maximum power point tracking system and an overall 25% system efficiency accounting for electronics and mechanical parasitics such as dissipation to heat.

In this simulation, only the magnetic suspension is assumed to be the primary damping mechanism of external excitation. The response acceleration of the unsprung mass can be monitored to determine the potential comfort level of the driver and passengers, as outlined by the guidelines in Table 1. In practical applications, the tyres and the sprung seats will also have damping effects. Therefore, the response acceleration simulated here is already a worst case scenario.

Table 1. Range of acceleration of the unsprung vehicle mass and the corresponding comfort levels as per ISO 2631-1 [30].

Acceleration (m/s^2)	Comfort Level
$\ddot{y}(t) < 0.315$	Comfortable
$0.315 < \ddot{y}(t) < 0.63$	A little uncomfortable
$0.50 < \ddot{y}(t) < 1.00$	Fairly uncomfortable
$0.80 < \ddot{y}(t) < 1.60$	Uncomfortable
$1.25 < \ddot{y}(t) < 2.50$	Very uncomfortable
$\ddot{y}(t) > 2.00$	Extremely uncomfortable

Assuming a comfort level of 0.315 m/s^2 as outlined in Table 1, the majority of the parameter space for the sinusoidal simulation fits within this threshold. It will be demonstrated later that 0.1 Hz–10 Hz is a good approximation for excitation frequency at varying vehicle speeds on a typical paved road.

3.2. Sinusoidal and Noise Simulation Results

Figures 5 and 6 illustrate the average response acceleration of the unsprung mass and maximum theoretical power recoverable from the suspension mechanism when subjected to sinusoidal excitations of varying frequency and acceleration amplitude. In real-world conditions, lower excitation frequencies ω would have very low acceleration amplitudes a, as the displacement amplitude A remains the same for a given road roughness profile. Assuming a sinusoidal model, this correlates to: $a(t) = -A\omega^2 \cos(\omega t + \phi)$, where ϕ is the phase angle.

The time domain example in Figure 6 shows that the response will trace the excitation frequency pattern for a harmonic excitation. However, real-world road irregularities rarely provide harmonic excitations, apart from a string of well spaced road bumps on smooth pavement. More realistically, the excitation tends to be noisy in nature.

Figure 7 presents an example of the system when it is subjected to band-limited (0 Hz–2 kHz) white noise with a noise intensity of 9.8×10^{-4} g^2/Hz. The zoomed view illustrates that the suspension

system oscillates and decays at its own nonlinear magnetic spring natural frequency as it damps out the external vibration. The average power recoverable in this example was 3.7 kW, with instantaneous peaks attaining 15 kW.

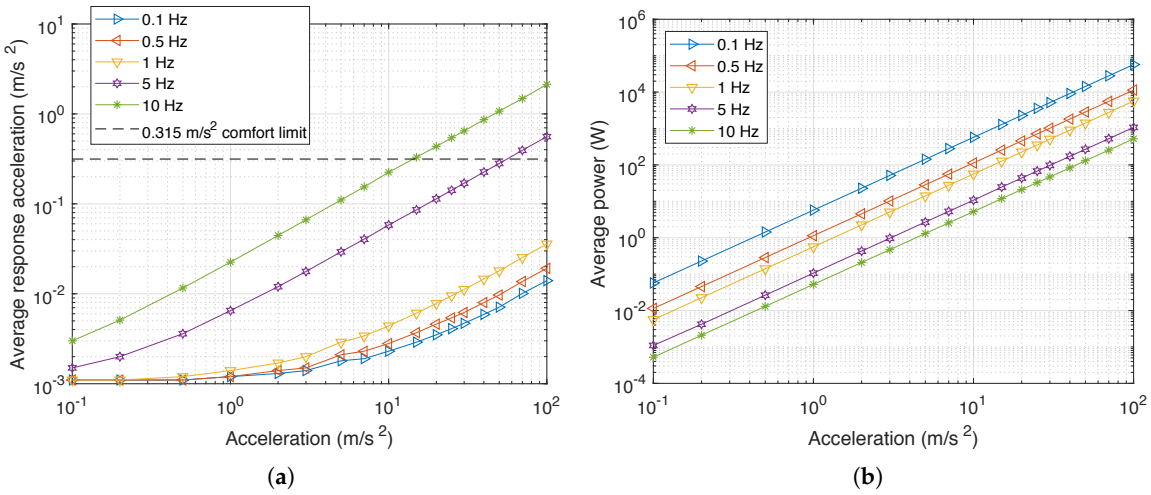

(**a**) (**b**)

Figure 5. The average response of the magnetic suspension when subjected to sinusoidal excitation between 0.1 Hz and 10 Hz, as well as between 0.1 m/s^2 and 100 m/s^2. (**a**) Response acceleration (comfort level); (**b**) recoverable power from suspension.

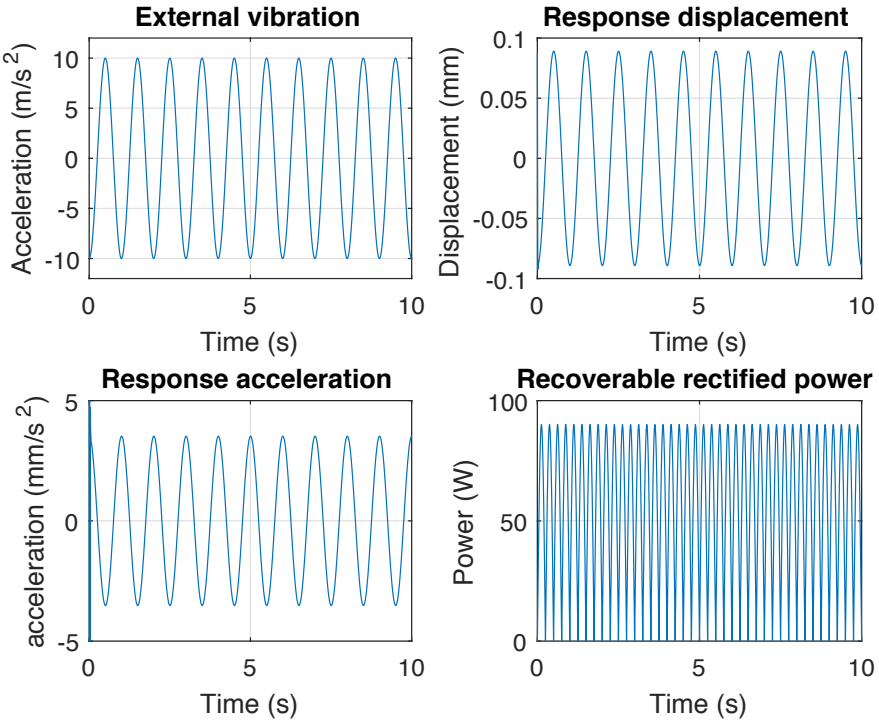

Figure 6. Time domain response of the magnetic suspension and the unsprung mass when subjected to a sinusoidal excitation of 10 m/s^2 at 10 Hz.

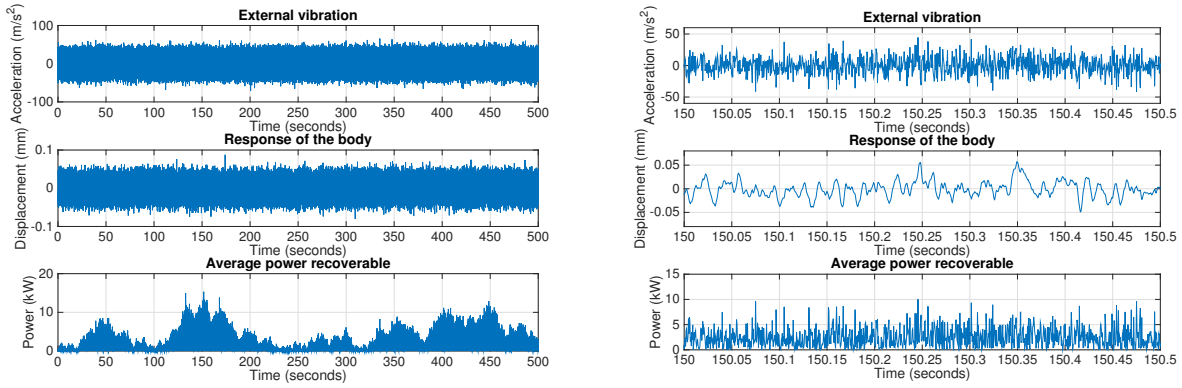

(**a**) (**b**)

Figure 7. Input and response when subjected to band-limited (0 Hz–2 kHz) white noise with a noise intensity of 9.8×10^{-4} g^2/Hz. (**a**) View over 500 s; (**b**) zoomed view for 0.5 s.

3.3. Measured Road Condition Simulation Results

However, to be more realistic, real road roughness data were further used to simulate the response behaviour. Data from an Australian road near Brisbane [31] was used for the simulation. These data were recorded and published by the Queensland Government and quantify road roughness in terms of the International Roughness Index (IRI).

The IRI is a standard metric used to quantify rough irregularities by measuring longitudinal road profiles [32]. Most paved roads have an average IRI between 1.5 and 6.0 depending on varying imperfection conditions, and unpaved or damaged pavements might have an IRI varying between 3.5 and 20.0 [33]. A summary of road conditions of various types of roads and their corresponding typical IRI ranges are shown in Table 2.

Table 2. Typical road roughness conditions of various roads in terms of the International Roughness Index (IRI) [32,34].

IRI (m/km)	Example Road Type	Comment
<2.0	Airport runway and highway	
1.5–3.5	New pavements	Surface imperfections
2.5–6.0	Old pavements	Minor depressions
3.5–10.0	Maintained unpaved roads	Frequent depressions
4.0–11.0	Damaged pavements	
8.0–20.0	Rough unpaved roads	Deep depressions

The IRI profile of the Australian road is presented in Figure 8. The average IRI value for this road is 2.79 m/km, which corresponds to a typical paved road. However, as shown, the road does have two isolated instances of very large road depressions at 19.95 m/km and 13.45 m/km.

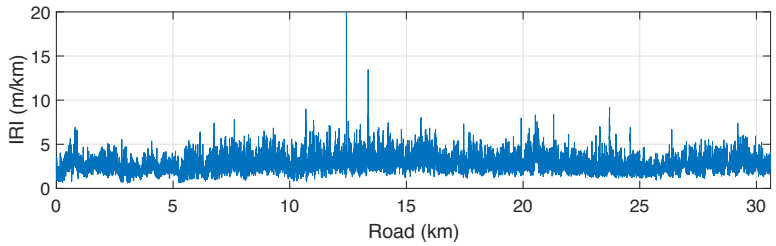

Figure 8. View of measured road condition data of an Australian road represented in the format of the International Roughness Index (IRI) [31]. The average IRI for this road is 2.79 m/km.

Depending on the vehicle speed, the quarter vehicle model will experience the road roughness features at varying frequencies, which then act as the external excitation acceleration. Figure 9 summarises the frequency of hitting a road irregularity feature (regardless of amplitude) on this road, as the vehicle drives on it between 1 km/h and 130 km/h.

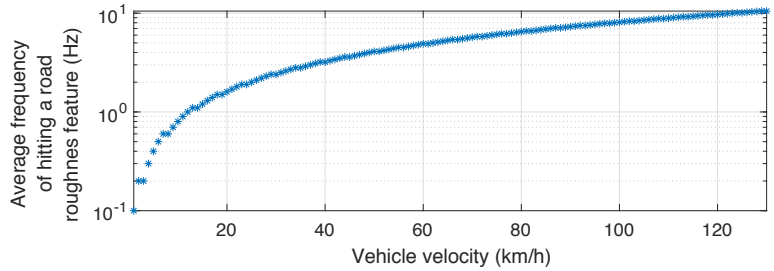

Figure 9. Average frequency of the vehicle hitting a roughness feature in the road condition data of an Australian road [31], estimated for varying vehicle velocities.

The IRI data were converted to acceleration data, for corresponding vehicle speeds. Typical urban vehicle speeds can be assumed to be in the range of 30 km/h–60 km/h, while those of extra-urban (highway/motorway) can be assumed to range around 100 km/h–130 km/h [35]. Figures 10 and 11 present the time domain simulation when the vehicle is travelling at 50 km/h on this road.

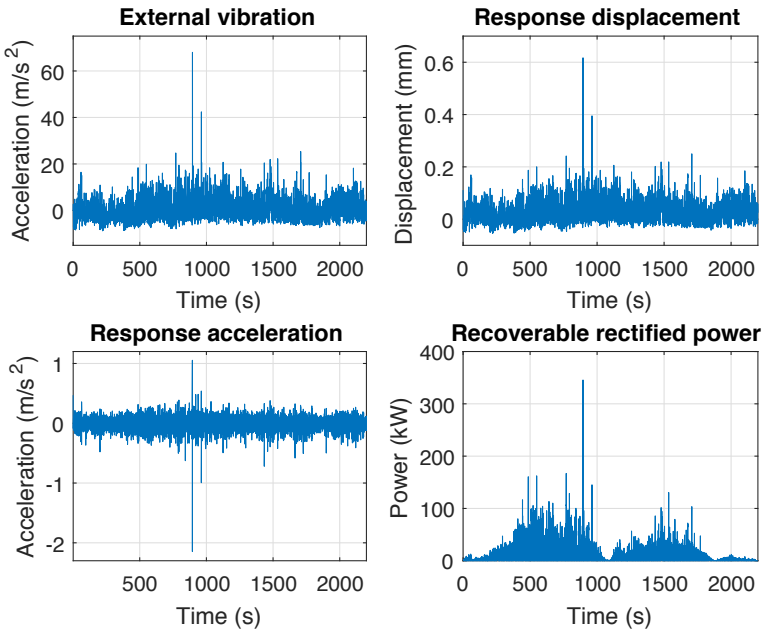

Figure 10. Time domain view of external vibration and response from one electromagnetic suspension on a wheel based on measured data from real road conditions with a vehicle travelling at 50 km/h.

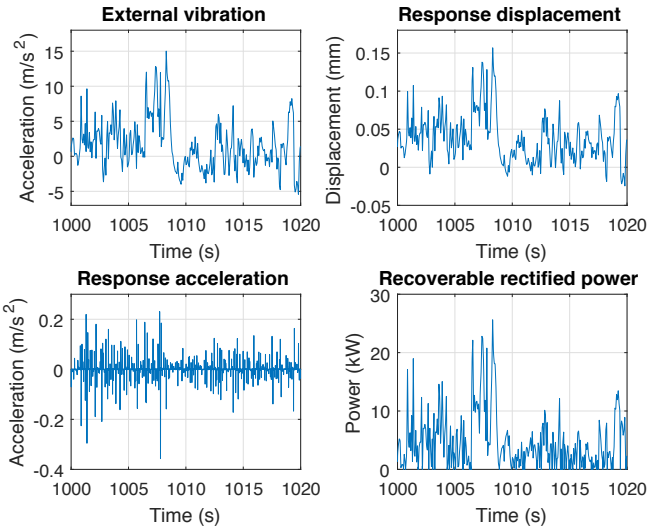

Figure 11. Zoomed view of external vibration and response from one electromagnetic suspension on a wheel based on measured data from real road conditions with a vehicle travelling at 50 km/h.

The average response acceleration is 0.0052 m/s^2 with frequent instantaneous peaks between 0.1 m/s^2 and 0.2 m/s^2. While this is well below the comfort threshold of 0.315 m/s^2, the isolated high road depression featured discussed earlier does result in an instantaneous response acceleration amplitude in excess of 2 m/s^2. However, in practical applications, the wheel damping effect and the sprung seat will be able to provide further cushioning.

The average recoverable power from the quarter vehicle model at the 50 km/h scenario is 10.48 kW. This corresponds to an average of over 40 kW recoverable across the entire vehicle. However, as seen in the time domain plots, the response is highly irregular, and the power electronics to harness the highly varying power peaks effectively (ranging between a few watts to a few hundreds of kilo-watts) would be a potential challenge. A possible solution could be the inclusion of an ultra-capacitor as an energy buffer, prior to the power management system, to recharge the onboard battery with the recovered power. However, a switch-based power conditioning system is required to maximise the efficiency.

Figure 12 and Table 3 summarise the average response acceleration and the average recoverable power of the quarter vehicle model when the vehicle speed is between 10 km/h and 130 km/h on the measured road roughness data.

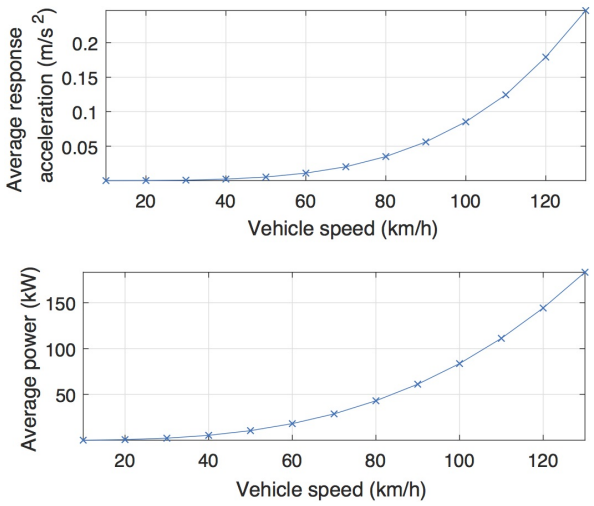

Figure 12. Average response acceleration and average recoverable power from one electromagnetic suspension on a wheel with varying vehicle velocities. Weight on top of one suspension assumed at 400 kg.

Table 3. Simulation result of the quarter vehicle magnetic spring model excited by measured road roughness road data at varying vehicle speeds.

Vehicle Speed (km/h)	Average Response Acceleration (m/s^2)	Average Recoverable Power (kW)
10	7.77×10^{-6}	0.08
20	1.37×10^{-4}	0.67
30	6.93×10^{-4}	2.26
40	0.0022	5.36
50	0.0052	10.48
60	0.0109	18.13
70	0.0201	28.74
80	0.0349	43.08
90	0.0561	61.15
100	0.0853	83.64
110	0.1245	111.20
120	0.1792	144.29
130	0.2467	183.32

It can be seen that up to 130 km/h, the average response acceleration is still below the 0.315 m/s^2 comfort threshold. However, the average value does not inform about the instantaneous peaks. Similar to the example from Figure 10, while the average might sit well within the comfort threshold, there might be occasional peaks of discomfort as the car hits severe depressions.

In the simulation so far, 400 kg has been used as the effective mass on the quarter vehicle magnetic suspension model. Therefore, the total unsprung mass is assumed to be 1600 kg, which corresponds to an average medium-sized car. Figure 13 presents the average response of the quarter vehicle model as the effective mass varies. This can represent either a small motorbike or a large commercial vehicle. Simulation for 50 km/h and 100 km/h were contrasted, to represent typical urban and extra-urban scenarios, respectively.

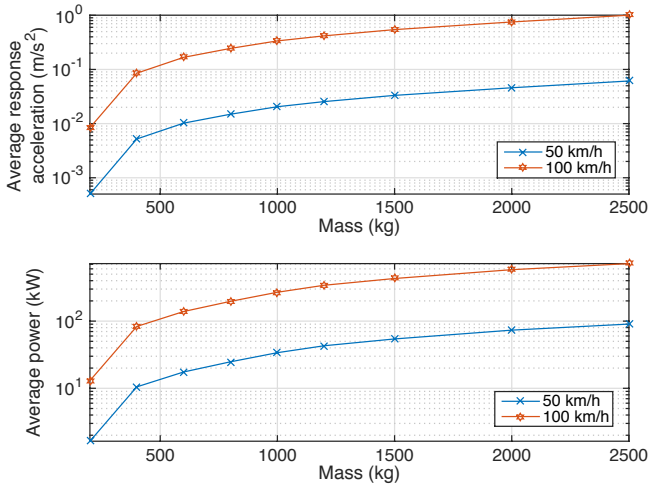

Figure 13. Average response acceleration and average recoverable power from one electromagnetic suspension on a wheel with varying mass on top of one suspension.

Unsurprisingly, as mass increases, the total power available also increases. However, this does come at the expense of the acceleration experienced by the unsprung mass. In large mass scenarios, multiple or larger magnetic suspensions would be needed to damp the external vibration. The larger power recoverable can then also be used to extend the range of a potential electrically-propelled lorry.

4. Discussion

The proposed magnetic spring suspension system is a fundamental suspension redesign, and it is intended to maximise the harvesting of kinetic energy from the suspension through primary electrical damping by the electromagnetic transducer as the main source of damping for road-induced vibrational energy. All the simulation results here take into account an effective 11% efficiency (as described by the various anticipated losses above) of recoverable electrical power in contrast to the total theoretical mechanical power available. Despite this relatively cautious efficiency estimate, the predicted average power levels are significant to recharge EV batteries for the purpose of extending range. For a medium-sized car of a total of 1600 kg unsprung mass, the numerically predicted average power was >100 kW while travelling in excess of 105 km/h and still maintaining well below the first comfort threshold of 0.315 m/s^2 experienced by the unsprung mass.

This power level is several orders of magnitude higher than the previously reported parasitic approaches for recovering energy from retrofitting conventional suspension systems. For example, Zuo et al. experimentally indicated that an average power of 19 W can be recovered from a conventional vehicle suspension at a speed of 48 km/h [26] while the maximum harvestable power was theoretically predicated at 7.5 kW [19]. Khoshnoud et al. [24] used a quarter vehicle model to predict around 40 W raw power at 108 km/h while not accounting for transducer efficiencies. Xie and Wang [22] studied the harvestable power by piezoelectric transducers on typical road roughness conditions, which numerically predicted up to 738 W. Furthermore, Sultoni et al. [23] experimentally measured 11.6 W from their electromagnetic transducer coupled to a conventional mechanical spring, and their theoretical simulation predicted up to 45 W. It can be noted that the predicted power from the fundamentally redesigned magnetic suspension system proposed here is about 2–3 orders of magnitude higher than these existing studies.

Furthermore, the order of magnitude of predicted maximum power recoverable for the proposed system is close to the power requirement for typical electric motors within EV's powertrains. For example, the Nissan Leaf MY 2016 has an 80-kW electric motor, and the Tesla Model S has a 581-kW combined electric motor [7]. Therefore, this work lays the foundation for designing a fundamentally new type of suspension mechanism for next generation hybrid vehicles and EVs, which has the potential to both extend range and complement user comfort.

5. Conclusions

This paper proposed a fundamental redesign of the vehicle suspension system. By adopting an electromagnetic suspension with permanent magnets as the primary restoring element, electromagnetic coupling can act as the main damping mechanism to harness the energy available in suspensions during driving. Furthermore, the high order magnetic spring can act as an effective shock absorber system and help to improve rider comfort for large excitation scenarios (high driving speeds on rough roads). Analytical and numerical models were constructed for a quarter vehicle magnetic suspension system, and measured road roughness data from an Australian road were used to simulate the behaviour and response. Simulation results suggested that average recoverable power in the range of 10's of kW to >100 kW was possible from the quarter vehicle suspension as the average response acceleration remained below the recommended comfort threshold of 0.315 m/s^2. Such a power level is about 2–3 orders of magnitude higher than previous reported regenerative suspension approaches that aimed to retrofit transducers to existing conventional suspensions. The results reported can potentially contribute towards the next generation of electric and hybrid vehicle designs, where the energy recovery system can effectively help to recharge the onboard battery while driving, as well as enhancing the comfort levels of the driver and passengers. Future work will involve proof-of-concept experimentation, as well as combining existing electromagnetic suspension control systems to further improve the user comfort levels.

Author Contributions: Y.J. and Y.S. devised the research and contributed to writing the manuscript. Y.J. built the analytical and numerical models. All authors (Y.J., Y.S. and S.L.) contributed to the discussion and reviewing of the manuscript.

Funding: No external funding was received for this research.

Acknowledgments: The authors would like to acknowledge the University of Chester for the institutional support of part of the research.

Conflicts of Interest: The authors declare no conflict of interest.

References

1. Lightweigting Working Group. *Lightweight Vehicles and Powertrain Structures: UK Opportunties*; Technical Report; Automotive Council UK: London, UK, 2013.
2. Ministery for Ecological and Inclusive Transition. *Climate Plan*; Technical Report; The French Government: Paris, France, 2017.
3. Department for Environment, Food and Rurual Affairs, Department for Transport. *UK Plan for Tackling Roadside Nitrogen Dioxide Concentrations*; Technical Report; The UK Government: London, UK, 2017.
4. *A Nation With Ambition: The Government's Programme for Scotland 2017-18*; The Scottish Government: Edinburgh, UK, 2017.
5. Pereirinha, P.G.; González, M.; Carrilero, I.; Anseán, D.; Alonso, J.; Viera, J.C. Main Trends and Challenges in Road Transportation Electrification. *Transp. Res. Procedia* **2018**, *33*, 235–242. [CrossRef]
6. Pearre, N.S.; Kempton, W.; Guensler, R.L.; Elango, V.V. Electric vehicles: How much range is required for a day's driving? *Trans. Res. Part C Emerg. Technol.* **2011**, *19*, 1171–1184. [CrossRef]
7. Fuel Economy and Environment Label. Available online: https://www.epa.gov/greenvehicles/explaining-electric-plug-hybrid-electric-vehicles (accessed on 6 November 2018).
8. Affanni, A.; Bellini, A.; Franceschini, G.; Guglielmi, P.; Tassoni, C. Battery choice and management for new-generation electric vehicles. *IEEE Trans. Ind. Electron.* **2005**, *52*, 1343–1349. [CrossRef]
9. Tie, S.F.; Tan, C.W. A review of energy sources and energy management system in electric vehicles. *Renew. Sustain. Energy Rev.* **2013**, *20*, 82–102. [CrossRef]
10. Hsu, P. Power recovery property of electrical active suspension systems. In Proceedings of the 31st Intersociety Energy Conversion Engineering Conference (IECEC 96), Washington, DC, USA, 11–16 August 1996; Volume 3, pp. 1899–1904. [CrossRef]
11. Mapelli, F.; Sabbioni, E.; Tarsitano, D. *Energy Recovering from Vibrations in Road Vehicle Suspensions*; Springer: New York, NY, USA, 2011; pp. 67–75.
12. Wang, R.; Tran, V.; Gu, F.; Ball, A. An investigation on energy recovery analysis of active suspension system. In Proceedings of the 19th International Conference on Automation and Computing, London, UK, 13–14 September 2013.
13. Dineshkumar, R.; Elengovan, C.; Manivannan, P. Design and fabrication of magnet and spring suspension in bicycle. *Int. J. Innov. Res. Sci. Eng. Technol.* **2015**, *4*, 124–127.
14. Xiao, Z.; Jing, X. Frequency-Domain Analysis and Design of Linear Feedback of Nonlinear Systems and Applications in Vehicle Suspensions. *IEEE/ASME Trans. Mechatron.* **2016**, *21*, 506–517. [CrossRef]
15. Liu, J.; Li, X.; Wang, Z.; Zhang, Y. Modelling and Experimental Study on Active Energy-Regenerative Suspension Structure with Variable Universe Fuzzy PD Control. *Shock Vib.* **2016**, *2016*. [CrossRef]
16. Cao, D.; Rakheja, S.; Su, C.Y. Roll- and pitch-plane coupled hydro-pneumatic suspension. *Veh. Syst. Dyn.* **2010**, *48*, 361–386. [CrossRef]
17. Cao, D.; Song, X.; Ahmadian, M. Editors'perspectives: road vehicle suspension design, dynamics, and control. *Veh. Syst. Dyn.* **2011**, *49*, 3–28. [CrossRef]
18. Xiao, Z.; Jing, X. An SIMO Nonlinear System Approach to Analysis and Design of Vehicle Suspensions. *IEEE/ASME Trans. Mechatron.* **2015**, *20*, 3098–3111. [CrossRef]
19. Zuo, L.; Zhang, P.S. Energy Harvesting, Ride Comfort, and Road Handling of Regenerative Vehicle Suspensions. *J. Vib. Acoust.* **2013**, *135*. [CrossRef]
20. Huang, B.; Hsieh, C.Y.; Golnaraghi, F.; Moallem, M. Development and optimization of an energy-regenerative suspension system under stochastic road excitation. *J. Sound Vib.* **2015**, *357*, 16–34. [CrossRef]

21. Yan, S.; Sun, W. Self-powered suspension criterion and energy regeneration implementation scheme of motor-driven active suspension. *Mech. Syst. Signal Process.* **2017**, *94*, 297–311. [CrossRef]
22. Xie, X.D.; Wang, Q. Energy harvesting from a vehicle suspension system. *Energy* **2015**, *86*, 385–392. [CrossRef]
23. Sultoni, A.I.; Sutantra, I.N.; Pramono, A.S. Modeling, Prototyping and Testing of Regenerative Electromagnetic Shock Absorber. *Appl. Mech. Mater.* **2014**, *493*, 395–400. [CrossRef]
24. Khoshnoud, F.; Zhang, Y.; Shimura, R.; Shahba, A.; Jin, G.; Pissanidis, G.; Chen, Y.K.; Silva, C.W.D. Energy Regeneration From Suspension Dynamic Modes and Self-Powered Actuation. *IEEE/ASME Trans. Mechatron.* **2015**, *20*, 2513–2524. [CrossRef]
25. Guo, S.; Liu, Y.; Xu, L.; Guo, X.; Zuo, L. Performance evaluation and parameter sensitivity of energy-harvesting shock absorbers on different vehicles. *Veh. Syst. Dyn.* **2016**, *54*, 918–942. [CrossRef]
26. Li, Z.; Zuo, L.; Luhrs, G.; Lin, L.; Qin, Y.-x. Electromagnetic Energy-Harvesting Shock Absorbers: Design, Modeling, and Road Tests. *IEEE Trans. Veh. Technol.* **2013**, *62*, 1065–1074. [CrossRef]
27. Gysen, B.L.J.; Paulides, J.J.H.; Janssen, J.L.G.; Lomonova, E.A. Active Electromagnetic Suspension System for Improved Vehicle Dynamics. *IEEE Trans. Veh. Technol.* **2010**, *59*, 1156–1163. [CrossRef]
28. van der Sande, T.P.J.; Gysen, B.L.J.; Besselink, I.J.M.; Paulides, J.J.H.; Lomonova, E.A.; Nijmeijer, H. Robust control of an electromagnetic active suspension system: Simulations and measurements. *Mechatronics* **2013**, *23*, 204–212. [CrossRef]
29. Williams, C.; Yates, R. Analysis of a micro-electric generator for microsystems. *Sens. Actuators A Phys.* **1996**, *52*, 8–11. [CrossRef]
30. International Organization for Standardization. *Mechanical Vibration and Shock—Evaluation of Human Exposure to Whole-Body Vibration—Part 1: General Requirements*; International Organization for Standardization: Geneva, Switzerland, 1997.
31. Transport and Main Roads. Road System Condition—Roughness 1km. Available online: https://data.qld.gov.au/dataset/road-condition-roughness-data-and-class-1km-segments/resource/d618ce2e-7d29-4569-97bd-d97bd5831924 (accessed on 6 November 2018).
32. Sayers, M.; Gillespie, T.; Paterson, W. *Guide Lines for the Conduct and Calibration of Road Roughness Measurements*; Technical Paper 46; World Bank: Washington, DC, USA, 1986.
33. Elghriany, A.; Yi, P.; Liu, P.; Yu, Q. Investigation of the effect of pavement roughness on crash rates for rigid pavement. *J. Trans. Saf. Secur.* **2016**, *8*, 164–176. [CrossRef]
34. Giuseppe, C.; Giuseppe, L. Road Roughness and Whole Body Vibration: Evaluation Tools and Comfort Limits. *J. Trans. Eng.* **2010**, *136*, 818–826.
35. Department for Transport. Vehicle Speed Compliance (SPE01). Available online: https://www.gov.uk/government/statistical-data-sets/spe01-vehicle-speeds (accessed on 6 November 2018).